J. Fluid Mech. (1990), *vol.* 215, *pp.* 61–84
Printed in Great Britain

Visualization of longitudinal convection roll instabilities in an inclined enclosure heated from below

By J. N. SHADID[1] AND R. J. GOLDSTEIN[2]

[1] Sandia National Laboratories, Albuquerque, NM 87185, USA

[2] Department of Mechanical Engineering, University of Minnesota, Minneapolis, MN 55455, USA

(Received 13 January 1989 and in revised form 4 September 1989)

Experiments have been performed on the stability of buoyancy-driven flows of a high-Prandtl-number fluid in an inclined rectangular enclosure. Visualization of the stable planform of convection for various Rayleigh numbers and inclination angles is provided by a temperature-sensitive liquid crystal and gold-coated film heater assembly which serves as the lower surface of the enclosure. This assembly produces a nearly constant heat flux surface with a thermal conductivity of the same order as that of the test fluid. The results indicate that for large angles of inclination from the horizontal a steady transverse roll(s) structure is stable. As the angle of inclination is decreased steady longitudinal rolls replace the transverse roll(s) and for low angles a steady square-cell convection planform is observed. A region of unsteady wavy longitudinal rolls is also observed at sufficiently high Rayleigh numbers for low to moderate angles of inclination. In general the wavenumber of the longitudinal rolls increases with angle of inclination from the horizontal. Two distinct types of instability mechanisms are observed which modify the wavenumber of the longitudinal rolls: a cross-roll instability, which is a disturbance perpendicular to the original roll axis; and a pinching mechanism which combines two neighbouring longitudinal roll pairs into a longer wavelength roll pair.

1. Introduction

Horizontal and inclined fluid layers heated from below are simple hydrodynamic systems which model physical phenomena in such diverse fields as meteorology, astrophysics, geophysics, industrial processing, and energy conversion and conservation systems. In addition to various physical applications, buoyancy-driven flows are increasingly studied to yield insights into the transition process from laminar to turbulent flow. A major distinguishing feature of the onset of convection in inclined layers, as contrasted to horizontal layers, is the existence of a mean shear flow for the inclined case. Due to the gravity component parallel to the inclined heated surface, the onset of convection is in the form of longitudinal rolls aligned with the direction of inclination. This unique orientation of convection rolls contrasts with the random orientation of convection rolls found in an infinite horizontal layer. In this connection it has been suggested (Clever & Busse 1977) that transition to a three-dimensional form of convection in an inclined layer is an even more significant step in the development toward turbulence than in a horizontal layer. In the past decade a number of review papers have appeared on thermal convection in horizontal

fluid layers. Busse (1981) considers the transition to turbulence in Rayleigh–Bénard convection; Palm (1975) and Busse (1978) review the nonlinear properties of thermal convection; and Koshmieder (1974) presents a critical comparison of experimental results with theoretical studies. Over the years the following general picture of convective motions in a laterally unbounded layer of a high-Prandtl-number fluid confined between infinite, horizontal, isothermal planes has developed. As the Rayleigh number (dimensionless temperature difference) is increased slowly, the motionless state becomes unstable and convective motions begin when the stabilizing effects of thermal conduction and viscous friction are overcome by the destabilizing effect of the buoyancy force. Above this critical Rayleigh number of about 1708, motion commences in the form of hexagonal cells in all real fluids due to non-Boussinesq effects. When the departure from the Boussinesq assumptions is small, hexagonal cells soon are replaced by rolls at a Rayleigh number slightly above the critical value. As the Rayleigh number is increased further, another transition to a three-dimensional form of convection called bimodal convection occurs at a Rayleigh number of about 20000. Still further increases in the Rayleigh number will result in the transition to complex time-dependent motions and subsequently to turbulent flow at much higher Rayleigh numbers (Busse & Whitehead 1971 and Busse 1978).

In contrast to the perfectly conducting isothermal boundary case, real boundaries with thermal conductivities of the same order as or less than that of the fluid are predicted to exhibit very different features at the onset of convection. Using linear stability analysis, Sparrow, Goldstein & Jonsson (1964) and Hurle, Jakeman & Pike (1967) determined the decrease of the critical Rayleigh number with thermal conductivity ratio ζ of boundary conductivity to fluid conductivity. They also found that the wavenumber of the most unstable mode tends to zero as ζ approaches zero. Busse & Riahi (1980) and Jenkins & Proctor (1984), considered three-dimensional finite-amplitude convection for poorly conducting boundaries. Jenkins & Proctor (1984) show that the preferred planform of convection is square cells for $\zeta \leqslant O(1)$. Riahi (1985) considered asymmetry in the upper and lower thermal conductivity ratios, determining the domain for square-cell planform and two-dimensional rolls.

DeGraff & Van der Held (1953) were apparently the first to study inclined-layer convection between highly conducting boundaries. They observed that the non-uniqueness of planforms exhibited for infinitesimal disturbances in a horizontal layer was broken at non-zero angles by a unique orientation of convection rolls in the upslope direction (i.e. longitudinal rolls).

Hart (1971*a*, *b*) carried out a linear stability analysis, along with experimental measurements and observations using air and water to study flow in differentially heated inclined enclosures of aspect ratios (A_x, A_z) of (25, 11.7) and (37, 17.2). Here A_x is the ratio of length, W, in the X (upslope) direction to the height of the fluid layer, L. A_z is defined similarly with the length, D, in the Z (cross-slope) direction as shown in figure 1. Hart observed both longitudinal rolls (rolls with axis parallel to the upslope direction) and transverse rolls (rolls with axis parallel to the cross-slope direction). At sufficiently high Rayleigh numbers he observed unsteady wavy motion and a breakup of longitudinal rolls for inclination angles from the horizontal, between 5° and 70°. For Rayleigh numbers, Ra, less than $\approx 10^6$ the angle of inclination, Θ, from the horizontal was varied from 0° (hot lower plate) to 180° (hot upper plate). The planform of convection was determined by introducing small thin flakes of ground fish-scales into water and observing them from above through a glass top plate; velocity profiles were visualized using dye injected at strategic locations in the fluid. A stability map of the (Ra, Θ)-space along with photographs of

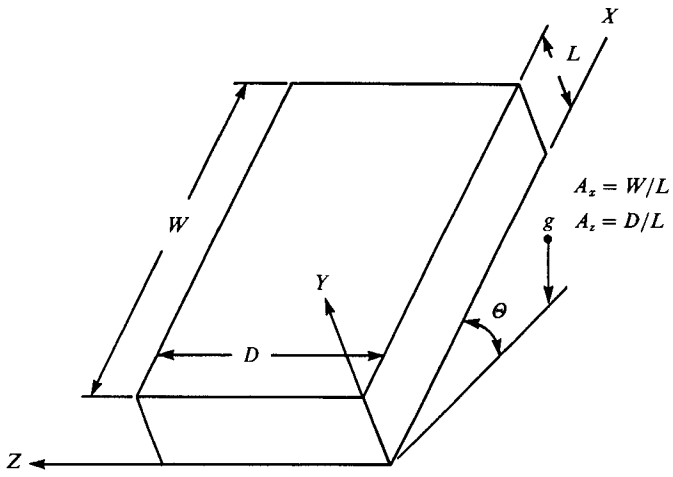

FIGURE 1. Inclined fluid layer heated from below and cooled from above.

the convective planforms were presented. A linear stability analysis of a parallel flow profile was used to predict the stability of the base flow to longitudinal and transverse modes; these results were compared to the experimental observations.

Clever & Busse (1977) presented a linear stability analysis to predict higher transitions of longitudinal convection rolls for Θ from 0° to 90°. They reported results for Prandtl numbers, Pr, of 0.71 and 7.0 corresponding to air and water respectively. At the higher Pr they found longitudinal rolls unstable to a cross-roll instability which acts perpendicular to the original roll axis, a wavy instability which is a standing wave on the original roll axis, and a transverse instability which acts at high angles of inclination.

Hassab & Ozisik (1981) & Hassab (1979) considered the effect of wall thermal resistance on the onset of cellular convective motion in a fluid confined in an inclined slot having very large aspect ratios. The parallel confining plates were subjected to convective boundary conditions on the outer surface of very thin (1979) and finite-thickness (1981) outer walls. They determined, by linear stability analysis, the onset of three types of instabilities occurring as longitudinal rolls, transverse rolls and travelling waves. The critical angle from the horizontal, Θ_{cr}, at which a transition occurs from longitudinal rolls to transverse rolls was found to vary from 72° for isothermal walls to 82° with constant heat flux boundaries, for $Pr = 0.72$.

The paper continues with a description of the experimental apparatus in §2. In §3, the observed convective planforms of motion are discussed. The planforms are similar to those identified by Hart (1971*a*, *b*) with the exception that at low angles of inclination, transverse disturbances perpendicular to the roll axis are stable. With the layer horizontal, square-cell planforms are the stable planform. The existence of such stable square cells is thought to be a consequence of the low thermal conductivity ratio, ζ, for the bounding surfaces. In §4 the cross-roll and pinching instabilities which change the wavenumber of planforms are discussed. These instabilities are similar to those observed by Chen & Whitehead (1968) and Busse & Whitehead (1971), for a horizontal layer between highly conducting boundaries.

2. Experimental apparatus

The liquid crystal/film heated assembly forming the lower heating surface ($Y = 0$ plane) of the inclined enclosure is shown in figure 2. This assembly provides an effective means of producing a nearly constant heat flux at the lower surface while at the same time allowing the temperature distribution on the surface to be easily visualized through the colour variation of the liquid crystal.

2.1. *Liquid crystals*

Liquid crystals have been used in several heat transfer studies both for qualitative and quantitive results. Early discussions (e.g. Fergason 1968) deal with the physical nature, historical background and possible uses of liquid crystals. Castellano & Brown (1973*a*, *b*) and Englehart & Hewgley (1973), review the application of liquid crystals to thermal mapping. Goldstein & Timmers (1982) and Goldstein & Franchett (1988) applied the liquid crystal technique to the visualization and measurement of heat transfer to multiple and inclined impinging jets respectively. Hart (1983) used a liquid crystal sheet to measure the wavelength of convection rolls in a shallow differentially heated layer of mercury. Hippensteele, Russell & Stepka (1981) and Simonich & Moffat (1982) have evaluated the applicability of using a composite of a gold coated plastic sheet (film) and liquid crystal to determine heat transfer coefficients. Gold-coated film heaters have been used by investigators to reduce the temperature gradient smoothing effect of wall conduction in studies simulating constant-heat-flow boundary conditions. Baughn *et al.* (1984) evaluated such a gold film heater from its performance in three heat transfer studies. Liquid crystals belong to a small group of organic compounds which are known to exhibit a unique intermediate structure during the freezing and melting process. During the melting process, the non-isotropic crystalline structure partially collapses, producing intermediate liquid states with an ordered structure. Upon freezing from the initially isotropic liquid phase partial recrystallization reversibly produces these same non-isotropic ordered structures. The intermediate ordered structure is referred to as a liquid crystal phase. In addition, compounds or mixtures which exhibit such intermediate phases are also referred to as liquid crystals.

Castellano & Brown (1973*a*, *b*) separate liquid crystals into two major categories: thermotropic liquid crystals and lyotropic liquid crystals. A further classification of the thermotropic liquid crystals by molecular arrangement of the crystals produces two subdivisions: smetic and nematic liquid crystals. One set of nematic liquid crystals, with interesting and useful thermal–optical properties are the cholesteric liquid crystals used in this investigation. In the liquid crystal phase, the wavelength of light reflected and transmitted by such cholesteric liquid crystals is a function of the crystal temperature. The cholesteric liquid crystal structure is an ordered stacking of molecular layers of compounds composed of cholesterol. Each layer of molecules is rotated slightly from the plane below it creating a helical structure of molecular layers. It is the pitch angle (between layers) which enables the crystal to selectively reflect light; an increase in the crystal temperature changes the pitch angle, thereby changing the selected wavelength for reflected light. Below the solid–liquid transition temperature the liquid crystal exists as a transparent solid showing the background colour, usually black. As the temperature of the liquid crystal is increased past the solid–liquid transition temperature, the layer reflects mainly brownish-red light from incoming white light. As the temperature is increased further, the reflected light changes colour (orange to yellow to green) until it becomes

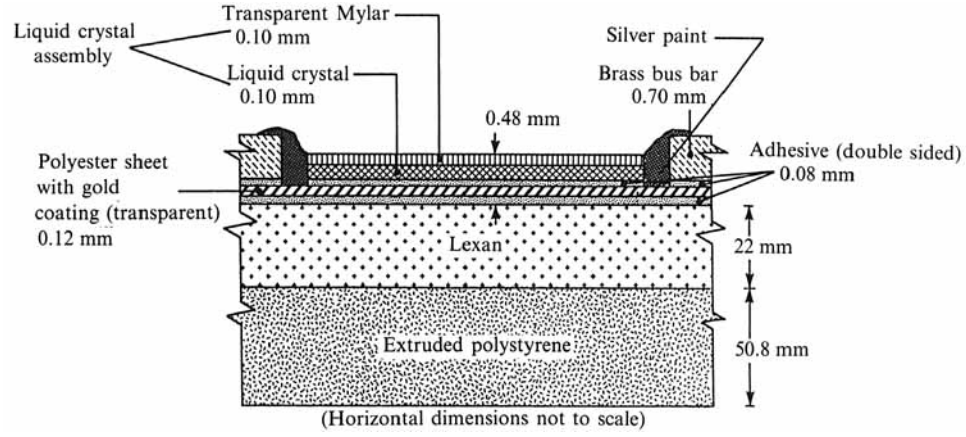

FIGURE 2. Schematic of the liquid crystal/film heater assembly.

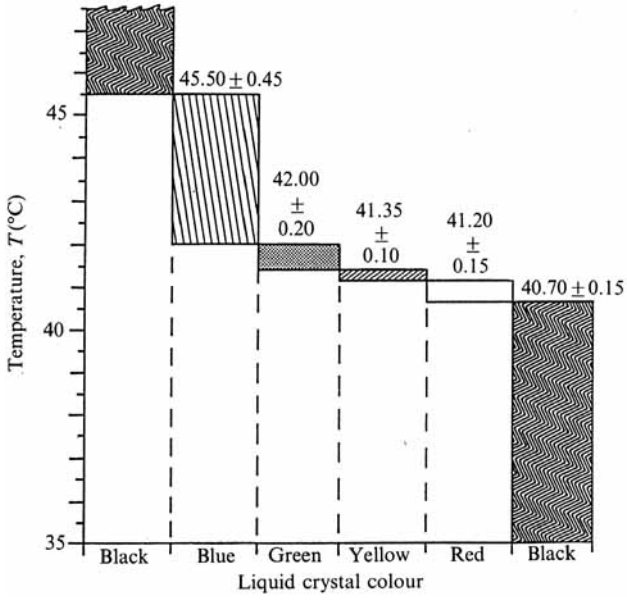

FIGURE 3. Typical calibration of cholesteric liquid crystal (values indicate one standard deviation of the mean).

blue. At still higher temperatures, the layer becomes an isotropic liquid and, as in the solid state, transparent showing the (usually black) background.

The particular liquid crystal used in the present experiment is manufactured by Liquid Crystal Applications Inc. (990 Raritan Rd. Clark, NJ 07066). The liquid crystal sheet consists of a thin (~ 0.10 mm) layer of liquid crystal with black ink background, covered on the top surface by a thin clear mylar sheet. This crystal undergoes its entire colour change from approximately 41° to 45 °C; a typical calibration for such a sheet is shown in figure 3. It is apparent from the calibration that accurate determination of temperature is available only at a transition point such as, for example, the red–yellow or yellow–green transition. Owing to its thin cross-section, the sheet has only small lateral heat conduction and a relatively short

(measured to be about $\frac{1}{2}$ s) thermal time constant. Thus, the liquid crystal has considerable usefulness in visualizing steady and mildly unsteady natural convection flows.

2.2. *Gold film heater*

A transparent, thin polyester sheet on which a gold coating has been vacuum deposited is used to provide a nearly constant-heat-flux boundary. This gold coating is thin enough to be semi-transparent to visible light and has negligible heat conduction along its surface. The wall conduction is essentially determined from the substrate upon which it is mounted. This property of the film heated allows a more accurate determination of the surface temperature distribution by minimizing thermal gradient smoothing effects common to other methods such as thin metallic sheet heaters. A simple calculation indicates that the ratio of lateral conduction losses for a 1/1000 in. stainless steel shim heater to a typical gold film heater is approximately 15.

The sheets used in this application were 0.12 mm thick with a gold-coating resistance of 16 Ω per square. The conducting gold layer is overcoated with a very thin ceramic coating in the manusfacturing process to protect the gold from abrasion. The manufacturer (Sierracin/Intrex Products (Sylmar, CA)) recommends a maximum heater load of approximately 1.2 kW/m^2 and a maximum operating temperature of 90 °C. We have operated the film at heat fluxes up to 1.4 kW/m^2 and at temperatures as high as 50 °C.

The uniformity of the heat flux produced by the gold film heater is influenced by the uniformity of the gold deposition, as well as the variation of resistivity of the coating with temperature. Indications are that the latter effect in our experiment is small since the sheet had a maximum variation in temperature of 7 °C. This corresponds to approximately a 1% change in resistivity (Baughn *et al.* 1984). The heater sections were cut from the central section of an 86 cm wide roll because of the increase in resistance as the edges of the sheet are approached. Measurements of resistance uniformity were made by applying a known voltage and current across the heater film and measuring the voltage drop from the bus bars to fixed distances on the film. These measurements indicate that the resistance of the film, along with the bus bar connection varied typically by 1% throughout the test region.

A composite of the above-mentioned liquid crystal and gold film heater forms the lower heated surface of the enclosure and is shown in figure 2. The liquid crystal sheet is affixed to the conducting surface (gold surface) of the film heater by an industrial double-side adhesive tape, except near the ends where the electrical connection to the bus bars is made. Two brass bus bars are fastened to the polyester film by the same double-sided adhesive and are electrically connected to the gold film heater by application of a silver-loaded paint. The energy dissipated in the film is conducted up through the liquid crystal and mylar plastic sheet, the top of which is in direct contact with the test liquid. When mounting the crystal to the heater, care is taken to eliminate trapped air pockets which could significantly increase the local resistance to heat flow through the composite. The liquid crystal/film heater assembly is then fastened to the Lexan substrate by a similar double-sided adhesive. The uniformity of such a composite assembly for flow visualization must be determined in place, and in this regard we refer to §3, where photographs of the liquid crystal surface, during actual tests, indicate a high degree of uniformity.

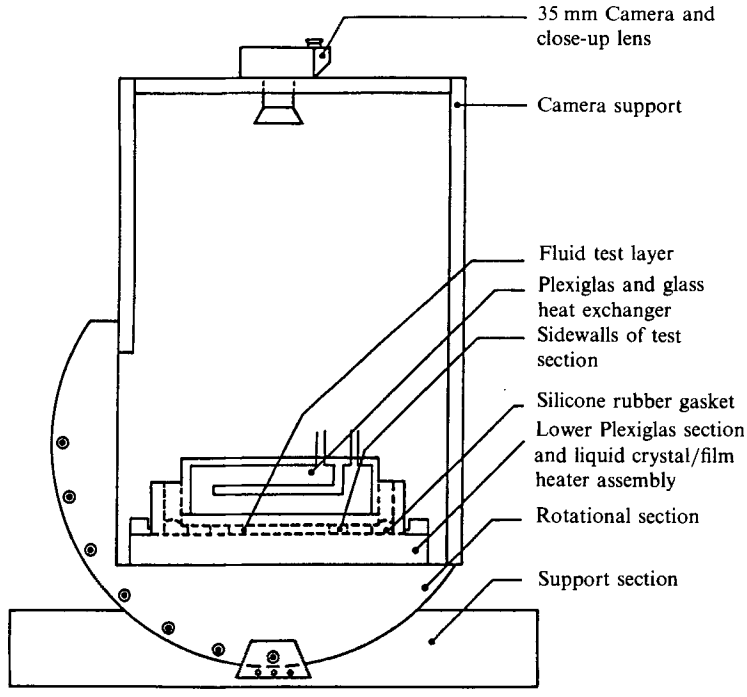

FIGURE 4. Schematic diagram of test apparatus for inclination of the enclosure.

2.3. *Inclined enclosure*

The experimental enclosure and the apparatus used to incline it, are shown in figure 4. The tilting mechanism consists of an adjustable rotational section and a stationary support section. A 35 mm camera used to photograph the liquid crystal surface is positioned directly above the centre of the test section on a camera support attached to the rotational section. The inclination angle is adjusted by sliding the rotational section on the circular arc runner of the support section. The two sections can be fixed together by a locater pin at 15° intervals, or clamped together for angles between any two pin positions. The inclination angle is determined using a bubble balance and protracter affixed to the camera support. The accuracy of this method for non-zero angles is $\pm 0.25°$ and for the zero angle $\pm 0.10°$. The deviation from horizontal of the axis of rotation is less than $\pm 0.075°$.

The test enclosure shown in figure 5 is formed below by an open box made of Lexan in which the liquid crystal/film heater assembly is mounted. Sidewalls of the desired aspect ratios (A_x, A_z) are placed over the central portion of the liquid crystal surface. Along the inner walls of the Lexan box, a silicone rubber gasket is used. The top of the test enclosure is a transparent Plexiglas and glass heat exchanger which is clamped down, sealing the test fluid within the confines of the gasket. Thus, the fluid fills both the test section, and the region between the sidewalls of the test section and the silicon rubber gasket. The lower surface of the transparent heat exchanger is a high-strength glass laminate of $\frac{1}{4}$ in. thickness; it is this glass plate which forms the upper surface of the test enclosure. This thickness of glass was necessary to withstand the pressure force acting on the glass during the process of sealing the gasket and removing excess fluid. Water from a constant-temperature circulator is passed through the heat exchanger at sufficiently high flow rates to obtain high convective

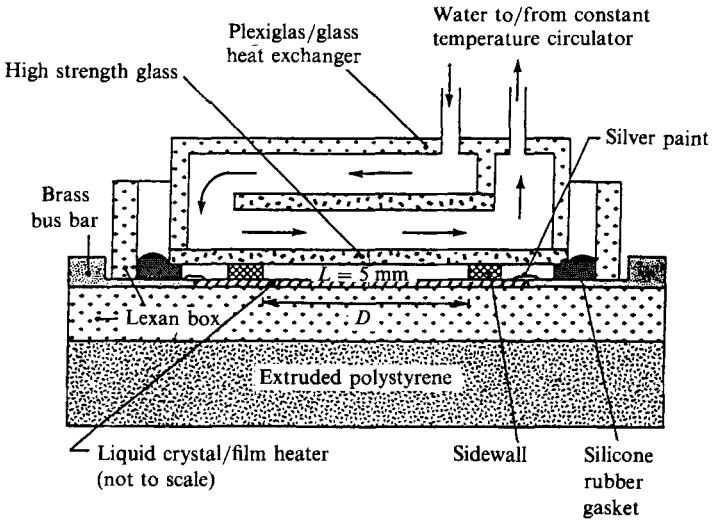

FIGURE 5. Cross-sectional view of test enclosure.

heat transfer rates, and ensure that the temperature increase of the cooling water is insignificant relative to the temperature difference across the fluid test layer.

Reagent grade ethylene glycol ($Pr = 90$) is used as the test fluid. The height of the fluid layer is 5 mm in all tests. The temperature difference across the fluid layer varies from about 2° to 10 °C, corresponding to kinematic viscosity variations of 4–25%.

The aspect ratios of the cells tested are various combinations of A_x and A_z with $1 \leqslant A_x \leqslant 20$ and $5 \leqslant A_z \leqslant 40$. The sidewalls used to form the test cells were either highly conducting (aluminium) or poorly conducting (Plexiglas). The placement of such walls on the lower surface is expected to disturb, locally, the nearly constant heat flux produced by the liquid crystal/film heater assembly. The effect of this non-uniformity for various aspect ratios on pattern-selection and on the various instabilities is discussed in §3.

In order to use the liquid crystal technique to visualize convection planforms, there must be a transparent optical path to the liquid crystal surface and, of course, a non-uniform temperature distribution along the liquid crystal surface itself. The high-strength glass plastic laminate forming the upper surface of the enclosure has a thermal conductivity estimated to be about two times that of the ethylene glycol (i.e. $\zeta \approx 2$), while the lower liquid crystal/film heater assembly surface has an estimated effective thermal conductivity about $\frac{3}{4}$ that of the test fluid (i.e. $\zeta \approx \frac{3}{4}$).

2.4. *Procedure*

The modified Rayleigh number, $Ra^* = g\beta q_w L^4/\nu\alpha k$, is used as a non-dimensional measure of the heat flux at the lower surface. In this definition, g is the gravitational acceleration, β the volume coefficient of thermal expansion, q_w is the constant heat flux at the lower surface, L is the height of the fluid layer, k is the fluid thermal conductivity, and ν and α are the diffusivities of momentum and thermal energy, respectively. A dimensionless time $\tau = t\alpha/L^2$ measures time, t scaled by the characteristic vertical thermal diffusion time, L^2/α, for the fluid layer. The calculated characteristic time for the 5 mm ethylene glycol fluid layer is on the order of 5 min. After filling the enclosure with the test fluid, cooling water is circulated through the upper surface cooling channel for a period longer than 50 thermal time constants to

ensure a uniform fluid temperature in the test enclosure before the onset of heating. This is true of start up for all Θ. In order to achieve controlled and reproducible initial heating conditions, a computer controlled, programmable power supply is used to ramp the voltage drop across the film heat at the desired rate. The voltage drop across the heater is stepped at 30 mV each 10 s to increase to the operating voltage in about 3 h.

Three different types of runs are conducted. The first type starts at $\Theta = 90°$ (vertical layer) and the angle, Θ, is decreased to $\Theta = 0$ (horizontal layer). Generally Θ is incremented in steps of about 5° at the higher angles; at lower angles increments of 2.5° and finally 1° are used. After each change in angle, photographs are taken of the time variation of planform, as the rolls rearrange to accommodate to steady-state conditions at the new angle. The time necessary for such rearrangement increases with decreasing angle and is discussed in §4. For some range of angles, sufficiently high Rayleigh numbers are found at which no steady planform is achieved. States are considered unsteady if they exhibit changing patterns of convection for more than 12 h (>140 thermal time constants). The second type of run starts at $\Theta = 0°$ and increases in angle to $\Theta = 90°$. A third group of runs takes place at various discrete angles of inclination ($0° \leqslant \Theta < 90°$) from the horizontal. In these, heating begins with the layer initially inclined and uniform in temperature. Sufficient time is allowed for the planform to become steady, or for a determination of the unsteadiness of the state to be made. Typically, runs of the first and second types last for 50–90 h, while runs in the third group are often shorter, with the exception of the 0° case, which can last up to 250 h. To make an approximate map of the stability regions for the various planforms it is experimentally expedient to use runs from the first and second groups since the angle of inclination is easily varied at a given Ra. Runs from group three are then used to verify the results from the group one and two runs. A summary of the experimental runs is presented in table 1. The possible existence of hysteresis effects on the wavenumber was evaluated and is discussed in §3.

3. Convective planforms of motion

The liquid crystal indicates the temperature distribution on the lower surface of the enclosure. It is from this temperature distribution that the corresponding flow structure is inferred. Typical temperature distributions for high and low angles of inclination are shown in figure 6 (Plate 1). The temperature distribution on the heated wall at high angles of inclination is essentially one-dimensional (figure 6*a*). The effect of the sidewalls is apparent from the non-uniformity of the red–yellow–green transition line near the walls. In this case highly conducting (aluminium) walls cause a local decrease in the liquid crystal temperature near the sides of the enclosure. This perturbation of the one-dimensional distribution extends about 5 mm (or one vertical height of the enclosure) from the sidewalls. Aside from that, at non-zero angles changing from insulating (Plexiglas) to conducting (aluminium) sidewalls has no visually discernible effect on the finite-amplitude flow structure, the wavelength data or the transition angles associated with the convective planforms. However, the direction of rotation for the rolls adjacent to the sidewalls is determined by the type of wall present. For insulating walls fluid rose near the walls, and for conducting walls fluid fell, owing to the temperature perturbations present from the walls.

For a horizontal layer, however, the temperature perturbation due to sidewalls

run no.	A_x	A_z	Type	T_{cw} (°C)	q_w[W/m^2]	$Ra^*/10^3$	Total time
108	5.1	20.5	1	24.0	1075	24.0	4
110	10	20.5	2	36.0	300	6.0	6
114	10	20.5	1,2	39.5	190	3.5	80
115	10	20.5	2	34.5	420	7.7	180
116	10	20.5	1	29.5	990	18.0	2
117	10	20.5	1	29.5	990	18.0	3
118	10	20.5	1	29.5	775	14.0	30
119	10	20.5	1,2	23.0	1200	21.5	12
120	10	20.5	1	29.5	775	14.0	50
121	10	20.5	1	22.5	1200	21.5	60
122	10	20.5	1	34.5	440	8.0	58
123	10	20.5	1	31.0	645	12.0	34
124	10	20.5	1	28.5	930	17.0	20
125	10	20.5	1	31.75	550	10.0	54
200	5	20	1	38.0	200	3.8.3	46
201	5	20	1	34.5	430	8.3	6
202	5	20	1	31.0	600	11.0	24
203	5	20	1	28.6	900	16.0	39
300	5	10	1	38.0	200	3.8	46
301	5	10	1	34.5	430	8.0	6
302	5	10	1	31.0	600	11.0	24
303	5	10	1	28.0	900	16.0	39
500	10	40	1	35.5	410	7.6	150
600.1	1	20	1	35.5	430	8.0	3
600.2	2	20	1	35.5	430	8.0	3
600.6	6	20	1	35.5	430	8.0	3
601.2	2	20	1	35.5	430	8.0	21
601.3	3	20	1	35.5	430	8.0	21
601.4	4	20	1	35.5	430	8.0	21
700*a*	10	20	3	28.5	750	14.0	50
700*b*	10	20	1,2	32.25	560	10.0	48
800	10	20	3	22.5	1200	22.0	14
900	19	20	1	35.0	430	8.0	190
5000	10	20	1,2	35.0	490	9.0	360

TABLE 1. Photographic runs: Fluid: reagent grade ethylene glycol ($Pr = 90$); depth of layer: $L = 5$ mm in all tests; T_{cw} (°C): cooling water inlet temperature

drives the convective motion near flow onset as rolls oriented parallel to the longer side. After steady state is reached the square-cell planform is always evident for all aspect ratios used. This forcing of rolls near onset is due to the wall-orientation effect on the normally random temperature fluctuations present in the fluid near onset. The fact that the square-cell pattern at $\Theta = 0$ is achieved for the steady states for both initially horizontal and initially inclined tests, along with the existence of square-cell planforms for all aspect ratios, indicates that the sidewall effect is not the controlling mechanism of finite-amplitude planform selection. Strictly speaking the characteristics of the motions near onset of convection in the horizontal layer are very difficult to determine by the liquid crystal technique. The fact that temperature perturbations exist near the sidewalls along with the inherent limitations of the liquid crystal to resolve (spatially) very small temperature gradients make determination of the onset of convection by observation of the finite-amplitude temperature distributions uncertain. The liquid crystal technique used is better suited for observation of finite-amplitude planforms of motion such as the square

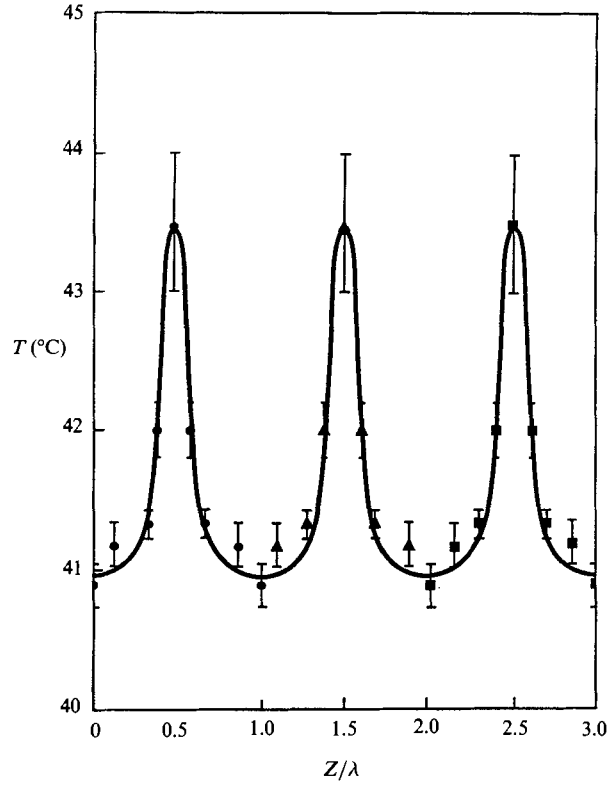

FIGURE 7. Longitudinal roll temperature distribution near the centre of the enclosure $(A_x, A_z) = (10, 20.5)$, $Ra^* = 10^4$, run no. 125.

cell, longitudinal roll and transverse roll structures. In general, these motions are accompanied by easily observable temperature variations using liquid crystals.

The uniformity of the liquid crystal/film heater assembly can be inferred from figure 6. In figure 6 (*a*) it is apparent that the temperature distribution on the heated wall is essentially one-dimensional, with the deviation from the one-dimensional distribution due to the above-mentioned effect of sidewalls. The uniformity of the heat flux distribution can also be inferred from the periodicity of the longitudinal rolls in figure 6 (*b*). The temperature difference from cool (brownish-red) falling liquid to warm (blue) rising liquid in each roll pair is approximately 5 K. A calibration of this liquid crystal, shown in figure 3, indicates an uncertainty of 0.1 K for the yellow–green transition line, or a relative uncertainty of 2% with respect to the temperature difference across the bottom surface of an individual roll. Therefore, if the actual temperature distribution for the longitudinal roll planform is indeed periodic, the visually observed regularity of the roll spacing in the spanwise direction substantiates the uniformity of the underlying heater/crystal composite. A plot of the measured temperature distribution at the midplane $X = \frac{1}{2}W$ across three roll pairs near the centre of the enclosure is shown in figure 7. The periodicity of the temperature distribution is clearly evident.

An approximate stability map of the (Ra^*, Θ)-space is presented in figure 8 for an enclosure of aspect ratio (A_x, A_z) of (10, 20). The locus of points separating regions of different planforms is determined by observation of finite-amplitude events and

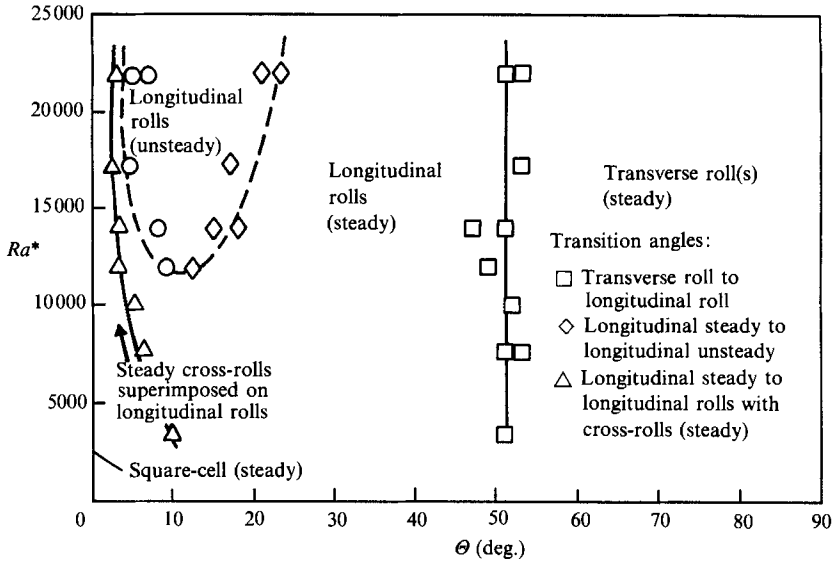

FIGURE 8. Approximate stability map. $(A_x, A_z) = (10, 20)$.

therefore can only be considered as approximating the true stability regions near the transition boundaries.

3.1. *Transverse mode*

At high angles of inclination from the horizontal, a steady transverse roll structure is stable. Figure 9(*a*) (Plate 2) is a typical liquid crystal representation for such an angle. The planform of motion is inferred from the essentially one-dimensional temperature distribution on the heated wall. The flow pattern corresponding to this temperature distribution is most likely non-unique since a unicellular flow, and a weak secondary multicellular flow superimposed on a unicell could conceivably produce the same temperature distribution on the heated wall. As in the case of isothermal walls, the existence of such motions would be dependent on Ra^* and the vertical temperature stratification. The existence of such transverse modes at high angles of inclination is in qualitative agreement with the observations of Hart (1971*a*, *b*) and the stability calculations of Hart (1971*a*) and Clever & Busse (1977) for isothermal boundaries.

As the angle of inclination is decreased, the transverse roll structure becomes unstable and below a critical angle, Θ_{cr}, it is replaced by longitudinal rolls, i.e. rolls with axes oriented in the upslope direction. This loss of stability to longitudinal rolls is known for the case of isothermal boundaries to be due to a shear instability (Hart 1971*a*; Clever & Busse 1977). Over the range of Ra^* tested, $3000 \leqslant Ra^* \leqslant 22000$, there is no discernible effect of Ra^* on Θ_{cr} (cf. figure 8). As the aspect ratio A_x is increased a corresponding increase in Θ_{cr} is apparent as shown in figure 10. This trend is qualitatively similar to the isothermal plate boundary condition situation. The aspect ratio A_z was found to have a negligible effect on Θ_{cr} for $10 \leqslant A_z \leqslant 40$ with $5 \leqslant A_x \leqslant 10$.

3.2. *Longitudinal rolls*

The longitudinal roll planform is characterized by a periodic variation of the temperature field in the cross-slope direction in addition to a non-zero temperature gradient in the upslope direction. The definition of the wavelength of such rolls is shown in figure 6(*b*). The wavelength λ of the longitudinal rolls is defined in terms

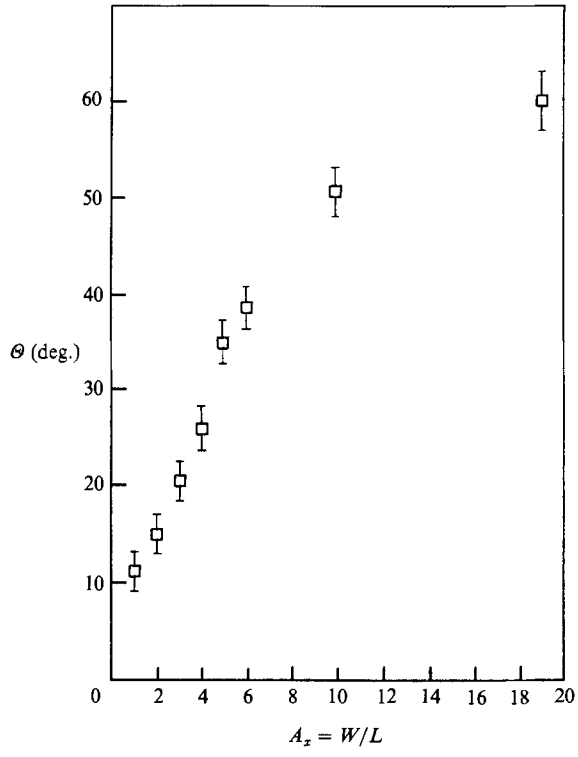

FIGURE 10. Effect of aspect ratio on the critical transition angle from longitudinal to transverse modes. $Ra^* \approx 10^4$, $A_z = 20$.

of a symmetric roll pair consisting of two counter-rotating rolls. On the liquid crystal surface, such a roll pair is determined by alternating hot or cold regions. The cold fluid which descends from the upper surface creates a low-temperature region on the crystal (seen as reddish-brown), whereas the hot rising fluid increases the local surface temperature (seen as green and blue colour). Thus the alternating cold or hot regions exist as roll boundaries between rolls having a reflection-type symmetry. The total number of roll pairs is determined by counting either the hot or cold regions periodically spaced in the cross-slope direction (the symmetric regions adjacent to each of the sidewalls are counted as one pair). At higher angles, Θ, the upslope temperature variation is noted to be larger than the corresponding roll-to-roll temperature variation resolved by the liquid crystal. This large variation in temperature is the reason why the liquid crystal surface loses its ability to resolve the roll planform near the lower and upper regions of the heated surface.

3.2.1. *Stability regions*

A typical sequence of photographs recording steady-state planforms at various angles of inclination for $Ra^* = 10000$ and $(A_x, A_z) = (10, 20)$ is presented in figure 9 (Plates 2 and 3). At 90° a transverse roll planform is evident. The colours vary from black (<40.7 °C) at the bottom where the cold descending fluid meets the heated surface, through the black–red (40.7 °C), red–yellow (41.2 °C), yellow–green (41.35 °C) and green–blue (42.0 °C) transition near the midline of the surface. Near the upper portion of the surface the liquid crystal undergoes its final colour transition

from blue to black (45.5 °C). The remainder of the surface has a temperature greater than 45.5 °C.

As the inclination angle is decreased through the critical angle a periodic cross-slope disturbance of the initially one-dimensional distribution becomes evident. The critical angle, Θ_{cr}, in this case is approximately 49°. This disturbance is first detected visually from the perturbation of the horizontal red–yellow–green transition line since the resolution of the crystal is highest in an interval about these transition temperatures. Such critical transition angles are measured for type-one and type-two runs (see §2.4); the standard deviation of the measured Θ_{cr} is $\pm 10\%$. At angles slightly below Θ_{cr}, the finite-amplitude disturbance is of sufficient contrast to photograph. Figure 9(*b*) shows the planform at 45.0° where it is apparent that a periodic cross-slope disturbance has been superimposed on the transverse planform. The temperature variation in this cross-slope direction is much smaller than the corresponding variation in the upslope direction. A further decrease in the angle of inclination causes a decrease of the temperature gradient in the upslope (X) direction, as evidenced by an increase in the length of the section of rolls resolved by the crystal (cf. figure 9*c*, *d*).

In general, the number of rolls in the enclosure is a non-decreasing function of the angle of inclination for angles less than Θ_{cr}. Then, as the angle of inclination is decreased, the number of rolls in the enclosure decreases as does the corresponding wavenumber of the planform. At 45° (figure 9*b*) there are 13 roll pairs present in the enclosure. As the angle is decreased from 35° to 30° a roll pair is lost to adjust to equilibrium conditions, leaving 12 roll pairs at the lower angle shown in figure 9(*c*). The planform at 15° appears essentially the same as at 30° except for the lengthening of the resolved rolls due to the decrease of the upslope temperature gradient. Upon decreasing the angle from 15° to 12.5° another roll pair is lost, leaving 11, when two roll pairs combine to form one pair of longer wavelength (figure 9*d*) by the pinching mechanism which is discussed in §4.2. The number of roll pairs present at 10° is evidently too large for equilibrium conditions at 7.5° for upon a decrease to that angle, an instability perpendicular to the original roll axis (termed the cross-roll instability) transforms the planform and replaces it with a lower-wavenumber planform (10 rolls) (figure 9*e*). The cross-roll instability along with the pinching instability are discussed in detail in §4.2. At 5° (figure 9*f*) nine roll pairs exist at steady-state with eight roll pairs found in the steady state at 2.5°; both changes are produced by the pinching mechanism. At the low angles of 5° and 2.5° (figure 9*f*, *g*) a periodic modulation of the longitudinal rolls in the upslope direction begins to be evident. This disturbance is perpendicular to the original roll axis and is approximately of the same spatial wavelength. The steady-state planform for a horizontal layer (figure 9*h*) appears to be a superposition of rolls with axis perpendicular to one another. Since $A_z/A_x = 2$, the eight rolls observed with axes in the Z-direction and four rolls with axes in the X-direction indicate that the average wavelength in the two directions is the same. This square-cell planform is discussed in detail in §3.3.

A region of unsteady motions exists for a range of angles, Θ, with $Ra^* \geqslant 10^4$ (cf. figure 8). These motions are of a quasi-periodic nature. This type of motion includes both a wavy motion and a periodic breaking and reformation of rolls. The form and period of such motions are discussed in §3.4.

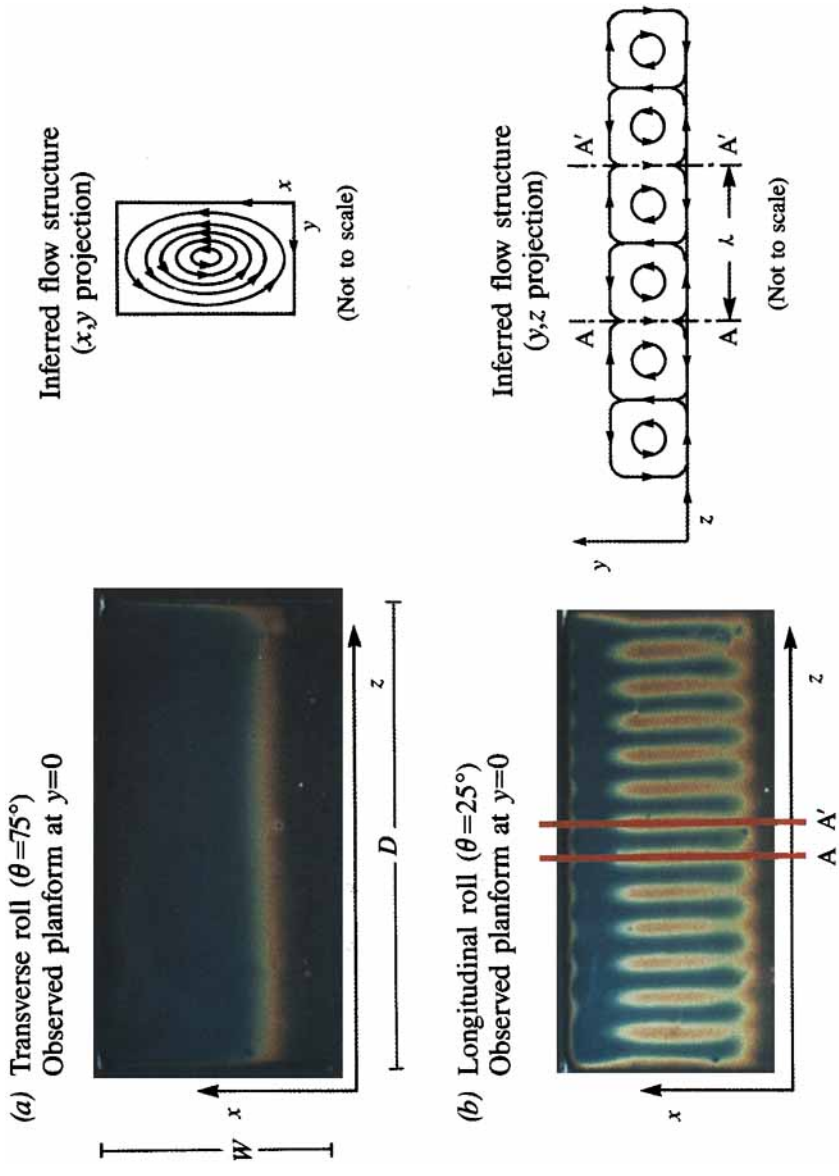

FIGURE 6. Interpretation of convective flow planforms: $(A_x, A_z)=(10,20)$, $Ra^*=10^4$, Run # 700b.

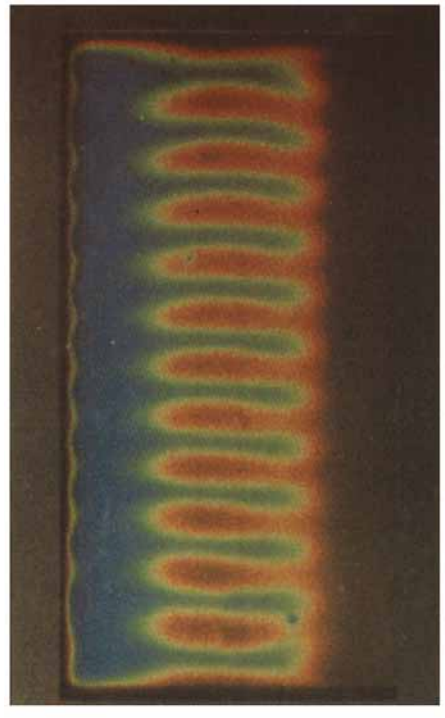

(c)

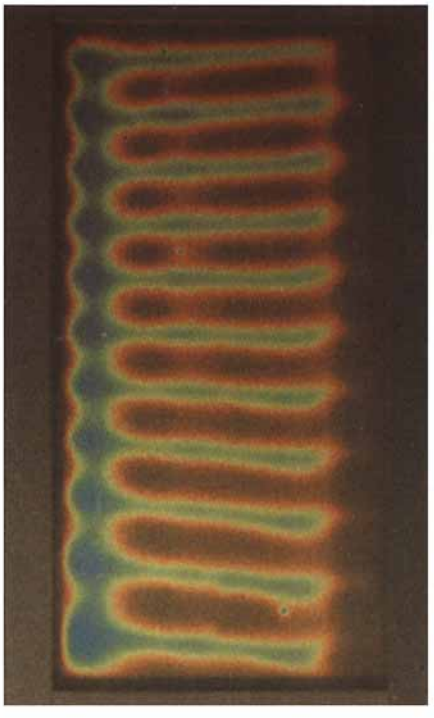

(d)

(a)

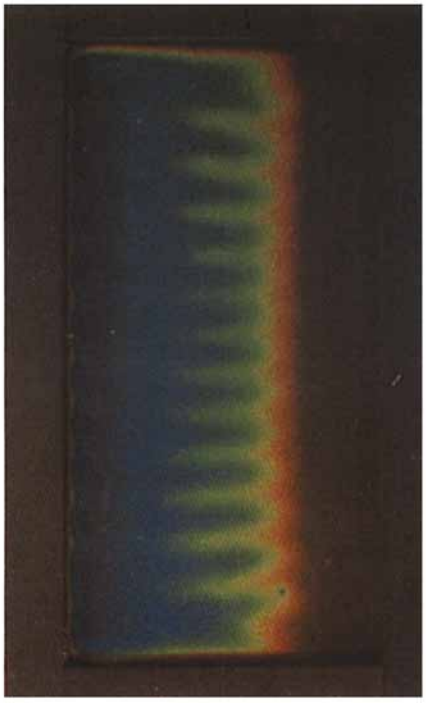

(b)

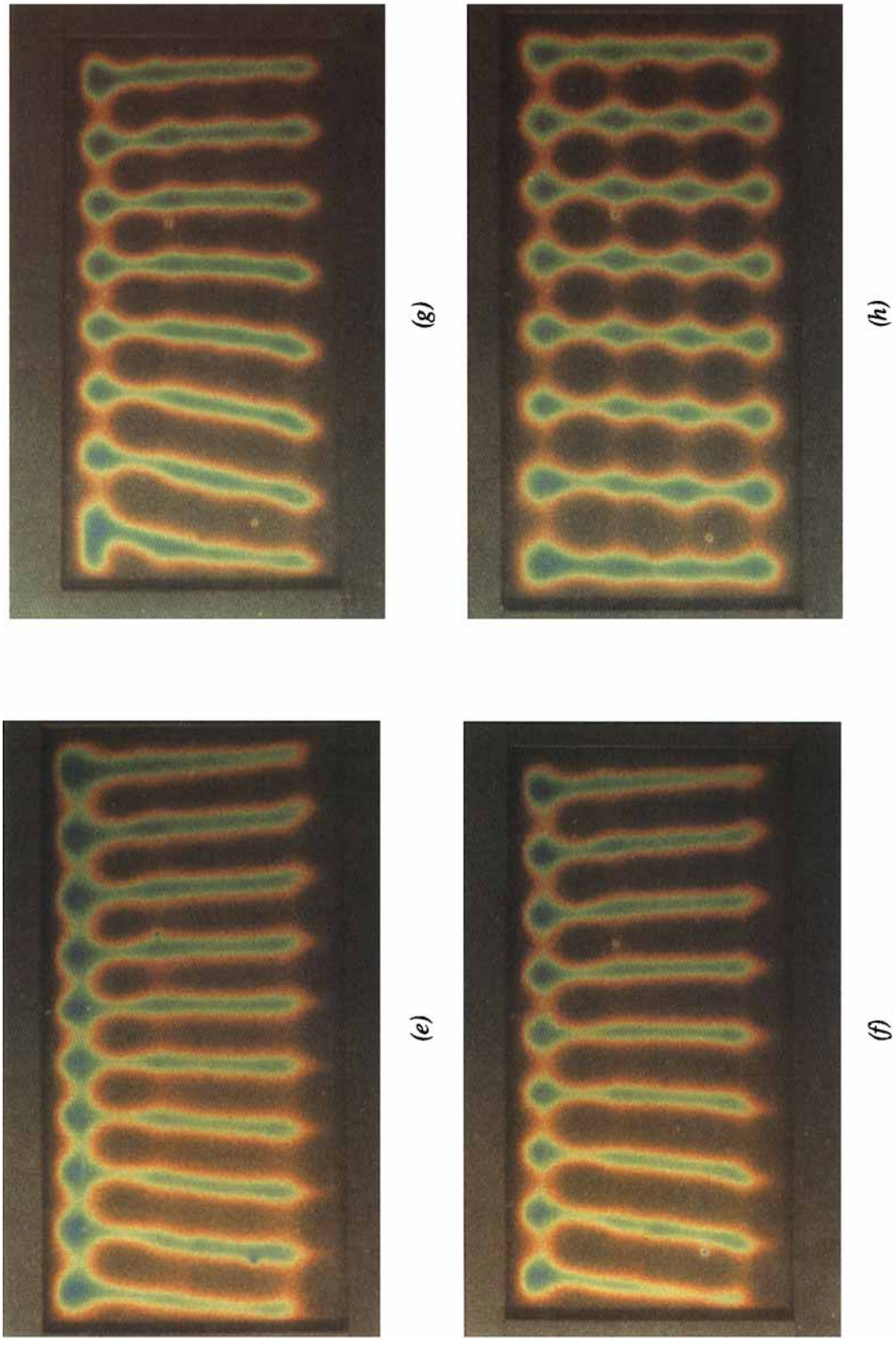

FIGURE 9. Typical sequence of liquid crystal surface photographs, from 90° to 0°: $Ra^*=10^4$, $(A_x,A_z)=(10,20)$, Run #700. *(a)* 90°, *(b)* 45°, *(c)* 30°, *(d)* 12.5°, *(e)* 7.5°, *(f)* 5°, *(g)* 2.5°, *(h)* 0°.

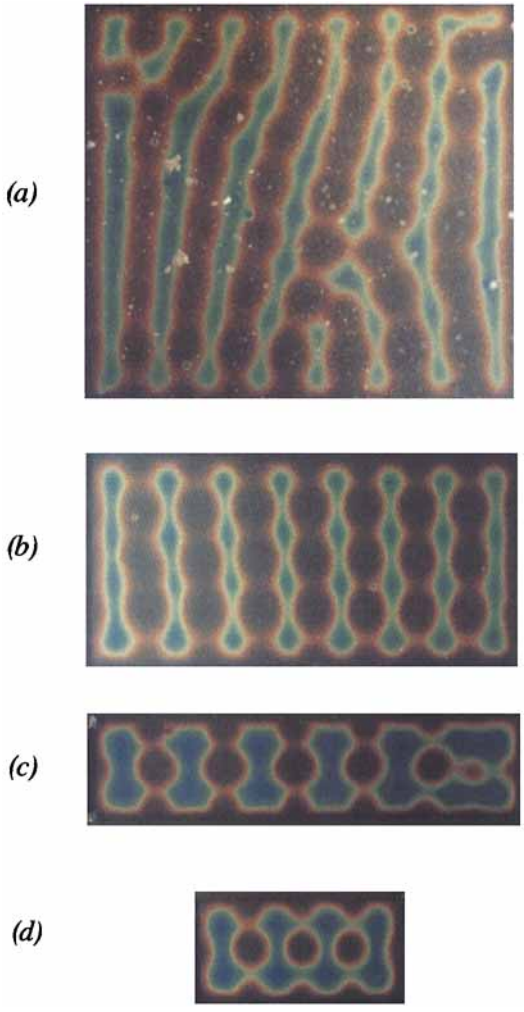

FIGURE 14. Photographs of square-cell temperature distributions for various aspect ratios. *(a)* $(A_x,A_z)=(19,20)$, $Ra^*=8\times10^3$, Run # 900; *(b)* (10,20.5), $Ra^*=10^4$, Run # 125; *(c)* (5,20), $Ra^*=8\times10^3$, Run # 201; *(d)* (5,10), $Ra^*=8\times10^3$, Run # 201.

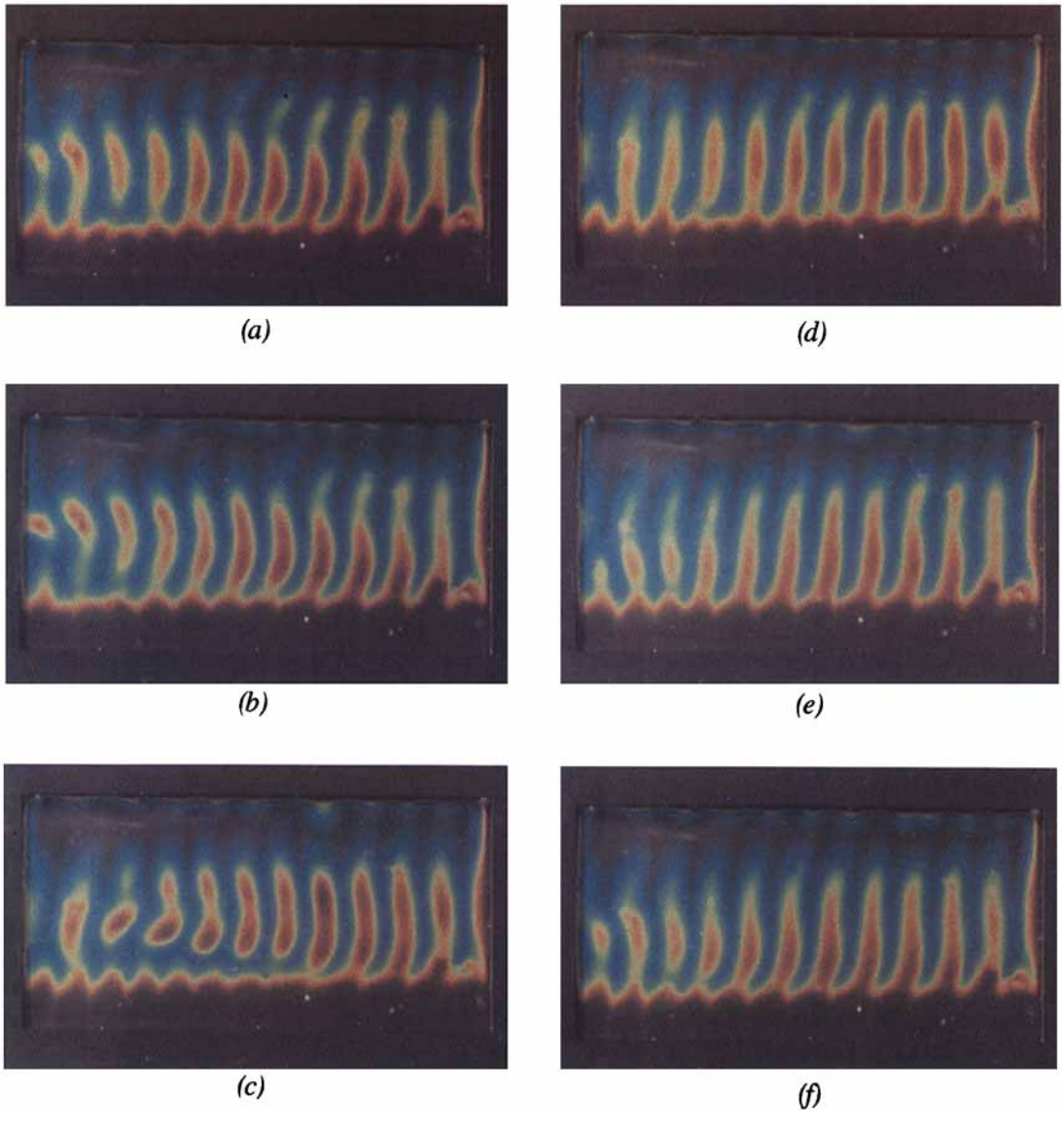

FIGURE 15. Photographs of unsteady wavy motion . $Ra^*=2.15\times10^4$, $(A_x,A_z)=(10,20.5)$, Run # 121 *(a)* $t=0$ min., *(b)* 1 min., *(c)* 4 min., *(d)* 5 min., *(e)* 8 min., *(f)* 10 min.

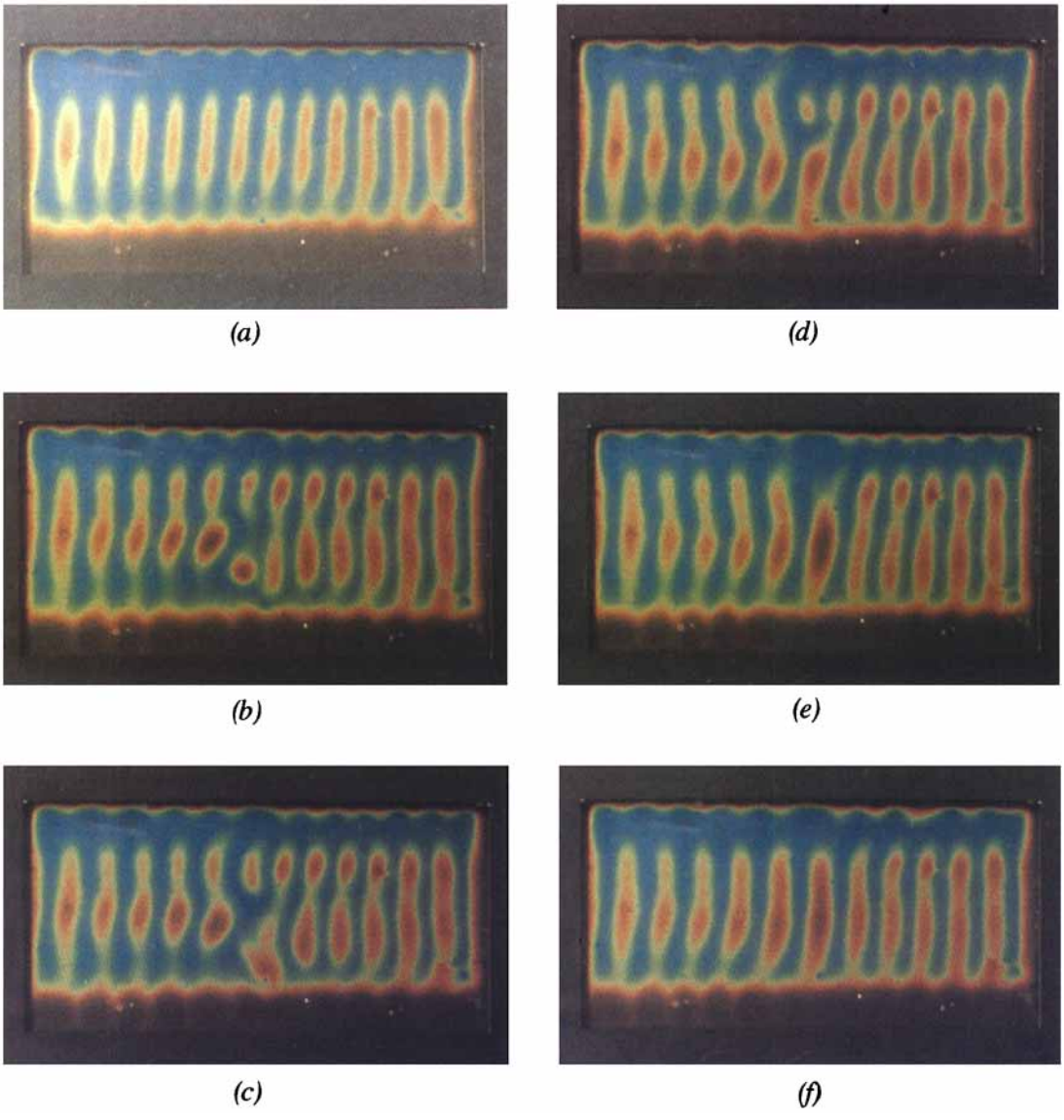

FIGURE 17. Pinching mechanism of roll-pair loss at 20°, $Ra^*=1.2\times10^4$, $(A_x,A_z)=(10,20.5)$, Run # 123 *(a)* $t=0$ min., *(b)* 1 min., *(c)* 3 min., *(d)* 3.5 min., *(e)* 5 min., *(f)* 8 min.

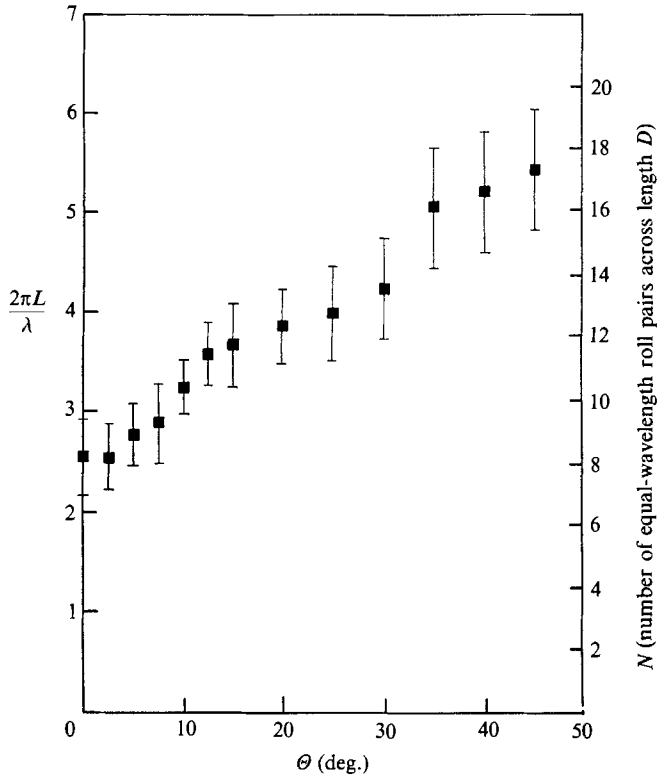

FIGURE 11. Inclination angle dependence on the wavenumber of longitudinal rolls for type 1 (Θ *decreasing*) runs. $(A_x, A_z) = (10, 20.5)$.

3.2.2. *Wavenumber data*

As mentioned above, the wavenumber of longitudinal rolls existing in the enclosure is a non-decreasing function of the angle of inclination from the horizontal. The results for runs from 90° to 0° for various Ra^* are presented in figure 11. The wavenumber is determined by measurements taken in the central 50% of the enclosure along the Z-axis. The dependence of the wavenumber on the angle of inclination is readily apparent. The dependence on Ra^* in the range studied, $3000 \leqslant Ra^* \leqslant 22000$, is small at most and is found to scatter within the uncertainty of the local wavenumber measurements for repeated runs at a constant Ra^*. The maximum uncertainty in the wavenumber measurements is about 18%. The wavenumber adjustments have been observed to occur in one of two ways: locally the wavenumber adjusts itself in various regions of the enclosure, for example smaller-wavelength roll pairs can exist at the sides of the enclosure and, globally, the wavenumber $\alpha = 2\pi L/\lambda$ is able to change by the loss of a roll pair. The latter was by far the most efficient mechanism that the planform used to decrease its wavenumber. The large uncertainty in the wavenumber measurements at a given angle is most likely due to a hysteresis-type effect of the change in angle on the planform wavenumber. This is seen clearly in figure 12 for $(A_x, A_z) = (10, 20)$. The upper limit of wavenumbers is associated with the type-one runs (Θ decreases), where it is evident that a delay in angle for the loss of a roll pair at a given angle is common. The lower limit of wavenumbers is produced from type-two runs (Θ increases), with an associated delay in the gaining of a roll pair at a given angle. The intermediate steady-state

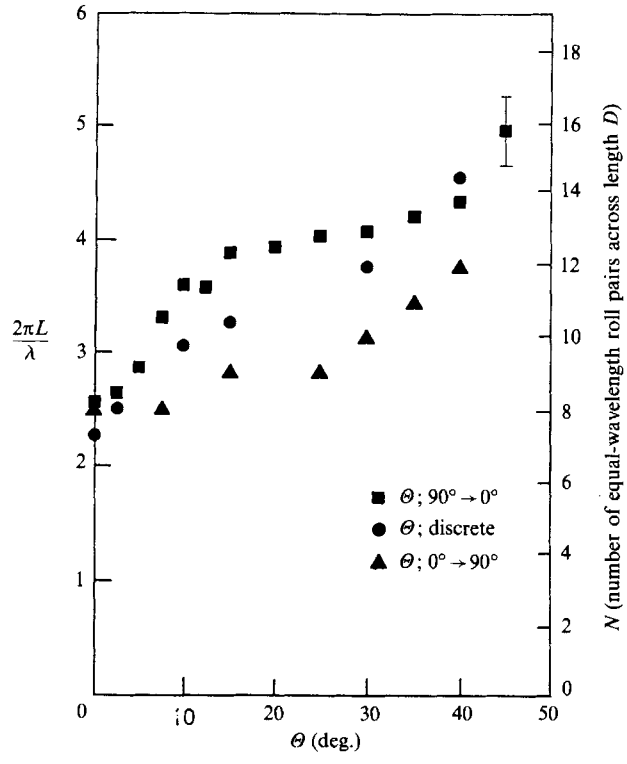

FIGURE 12. Hystersis effect of changes in angle of inclination upon the wavenumber of longitudinal rolls. $Ra^* = 1.4 \times 10^4$, $(A_x, A_z) = (10, 20)$, run no. 700*a*, *b*, *c*.

wavenumbers come from type-three runs in which heating starts at the given angle of interest. The type-one, -two and -three runs appear to converge to essentially the same limit of planform wavenumber at both high and low angles. The existence of discrete jumps in wavenumber (or number of roll pairs) as Θ increases or decreases is most likely due to the constraint of the finite aspect ratio A_z. These sidewalls effectively limit the number of roll pairs to an integral value (discrete wavenumber) at all times. This is in contrast to the possibility that a laterally infinite layer could sustain a continuous change in wavenumber as Θ is changed. The hysteresis effect in wavenumber with Θ could possibly be explained by the existence of a stable band of wavenumbers for a given angle; for a finite change in angle the stable band for two consecutive angles may overlap in the neighbourhood of the initially existing wavenumber. This overlap would then allow the existing wavenumber to lie in the stable regions for two consecutive angles without the need to lose a roll pair to change the wavenumber. Thus the angle at which the loss of the roll pair takes place would be determined by the value of the wavenumber for the previous angle, as well as the overlap of the stable wavenumber bands for any two given angles. The expected contribution to the total uncertainty of wavenumber for N roll pairs present in the enclosure as a function of angle, by this hysteresis effect alone, would then be approximately $1/N$. From figure 11 this would be about 10%, agreeing quite well for angles below about 25°. The deviation at higher angles is significantly larger and is probably due to the existence of smaller-wavelength roll pairs (near the sides of the enclosure) which were common at higher angles.

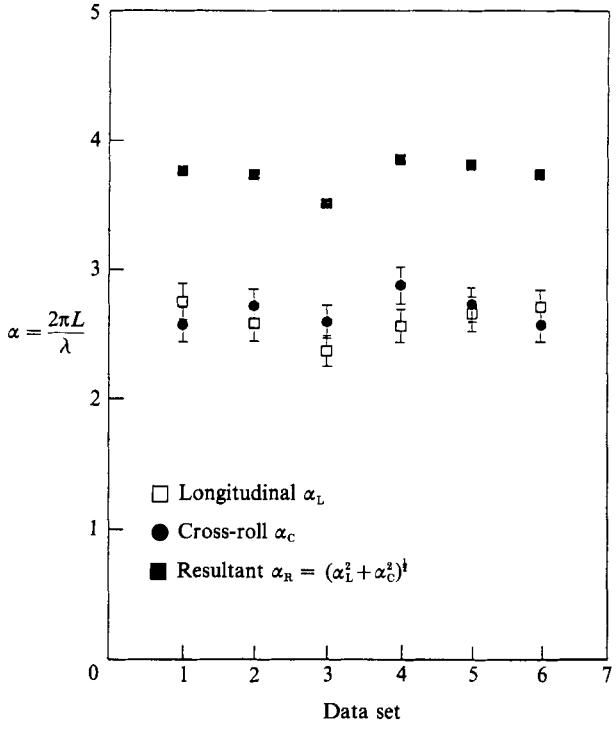

FIGURE 13. Comparison of component wavenumbers for square-cells at horizontal. (1) $(A_x, A_z) = (10, 20)$, $Ra^* = 8 \times 10^3$; (2) (10, 40), $Ra^* = 8 \times 10^3$; (3) (19, 20), $Ra^* = 8 \times 10^3$; (4) (10, 20), $Ra^* = 10^4$; (5) (5, 20), $Ra^* = 1.2 \times 10^4$; (6) (10, 20), $Ra^* = 1.6 \times 10^4$.

3.3. *Square-cell planform*

The square-cell planform found at $\Theta = 0°$ and the existence of steady perpendicular disturbances to the longitudinal rolls at small angles of inclination are thought to be due to the relatively low value for the thermal conductivity of the surface in comparison to that of the liquid layer. Busse & Riahi (1980) and Jenkins & Proctor (1984) predict that for surfaces of sufficiently low thermal conductivity, square-cells would be the stable post-critical planforms. Jenkins & Proctor (1984) determine this planform to be expected for thermal conductivity ratio $\zeta \leqslant O(1)$. In the present study this ratio is $\frac{3}{4}$ and 2 for the bottom and top surfaces, respectively. As mentioned above, the square-cell planform has been visualized for all aspect ratios and for both initially horizontal and initially inclined layers. The two component wavenumbers associated with the square-cell planform are plotted for various aspect ratios and Ra^* in figure 13, along with a resultant wavenumber. The wavenumbers of the two perpendicular components are essentially equal, which justifies the label 'square-cell' planform. Typical photographs of these planforms are shown in figures 9(*h*) or 14. Larger aspect ratios, as expected, are characterized by a much more non-uniform arrangement of cells, which is evident in figure 14(*a*) (Plate 4) where an initially inclined layer of aspect ratio (19, 20) is seen at horizontal. Throughout the layer, square-cells are evident but of a much less uniform distribution than in figure 14(*b*) for a layer of aspect ratio (10, 20). Planforms for enclosures with smaller aspect ratios of (5, 20) and (5, 10) exhibit the same type of square-cell pattern (figure 14*c*, *d*). Square-cells generated from initially horizontal layers, in general, are much more

random in orientation than square-cell planforms generated from initially inclined layers. In addition to orienting the square-cells, initial inclination appears to produce an amplitude asymmetry, with the Z-component (previously the longitudinal roll direction) having a stronger apparent circulation. This stronger circulation is inferred from the cooler temperatures of liquid crystal aligned along the previously inclined longitudinal direction as shown in figure 14(*b*).

Inclination of an initially horizontal layer also introduces an asymmetry into the square-cell structure. In the direction of inclination, the square-cell pattern is elongated, producing an increase in the component wavelength along the inclined direction. Conversely, as the angle of inclination is decreased (for initially inclined layers), a disturbance perpendicular to the longitudinal roll axis is generated; this disturbance has approximately the same wavelength as the square-cell component wavenumbers in a horizontal layer. This perpendicular disturbance to the original longitudinal rolls produces a steady cross-roll pattern at low angles of inclination and the steady square-cell pattern in the horizontal case. The approximate stability limit for this type of steady planform is shown in figure 8.

3.4. *Wavy and unsteady motion*

The unsteady motions present in the inclined enclosure are unsteady in a very restricted sense. For all inclined angles and Ra^* for which unsteady motions occur, a quasi-periodic variation of the planform with initial and final states of straight longitudinal rolls, separated by an approximately constant time period, is observed. Visual observations also indicate the possibility of two or more subharmonic frequencies existing in the cell. The term quasi-periodic is used to indicate that the intermediate planforms are not strictly repeatable; the motions, however, are similar from period to period with the initial and final states being essentially straight rolls. The term 'wavy' is used to describe a special case of periodic motions in which the rolls in their intermediate planforms bend their upper portions from side to side in a type of rhythmic swaying. This type of unsteady motion is similar to the wavy (travelling wave) disturbance observed by Hart (1971*a*, *b*). This wavy motion is not observed as often as the other forms of quasi-periodic motions, which include breaking and reformation of roll pairs and repeated destruction and creation of roll pairs.

An example of wavy motion is presented in figure 15 (Plate 5). The aspect ratios (A_x, A_z) are (10, 20), $Ra^* = 22000$, and the period of motion is about 10 minutes. In figure 15(*a*) it is apparent that the roll contains two bends with the tips bent to the right of the enclosure, as time progresses in figure 15(*b*, *c*, *d*, *e*) the rolls wave from right to left and finally back to the right (figure 15*f*). This wavy motion has been observed for more than 30 periods and found to remain essentially unchanged in its basic intermediate planforms.

4. Wavelength modifying instabilities

The fact that the wavenumber of longitudinal rolls is a non-decreasing function of the angle of inclination indicates that as the angle of inclination of the fluid layer decreases, mechanisms must exist to reduce the wavenumber of the longitudinal roll planform. Two distinct mechanisms have been observed: the cross-roll instability, which is a disturbance perpendicular to the original roll axis, and the pinching mechanism, which combines two neighbouring roll pairs into a longer-wavelength (smaller wavenumber) roll pair. These mechanisms have been exhibited for horizontal

layers between isothermal boundaries in the experiments of Busse & Whitehead (1971) and Chen & Whitehead (1968). In the inclined case, Clever & Busse (1977) have predicted a cross-roll instability for layers between isothermal boundaries with $Pr = 7$.

4.1. *Cross-roll instability*

The cross-roll instability acts perpendicular to the original roll axis. It has been observed to modify the existing wavenumber of the longitudinal rolls in at least two ways: causing a group of longitudinal rolls to break into multiple sections which later recombine to form a planform with a smaller wavenumber; and, at very low angles, the cross-roll instability leads to a steady square-cell planform. The wavenumber of the cross-roll disturbance is roughly equal to the component wavenumbers of the square-cells found at the horizontal (≈ 2.6) and independent of the wavenumber of the longitudinal rolls themselves. This correspondence of wavenumbers is not due to the formation of steady square-cell planforms, as it appears at angles at which no steady square-cell planforms have been observed. The longitudinal roll planforms, once reformed with a lower wavenumber, appear as before the onset of the instability. A typical rearrangement of longitudinal rolls upon decrease of the angle of inclination (in this case from 10° to 7.5°) is shown in figure 16. The cross-roll instability acts locally to decrease the number of roll pairs present, and at the final steady planform the wavenumber is found to be essentially uniform throughout the enclosure. The breaking-up of the roll pairs and their subsequent recombination proceed through a series of interesting and seemingly efficient movements. Over a period of 40 min., the planform has undergone the loss of a roll pair, and a global transient motion which produces a uniform cellular structure with a decreased wavenumber.

The cross-roll instability as a wavelength-changing mechanism is limited to $\Theta \leqslant 17°$. This dependence on angle is similar to the predictions of Clever & Busse (1977) who determined that disturbances at right angles to the longitudinal rolls are stabilized by the shear flow as the angle of inclination increases. At all but sufficiently low angles the cross-roll instability leads to the re-establishment of a longitudinal roll planform with a lower wavenumber. However, for very low angles, the cross-roll instability leads to a convection planform of square-cells upon decrease of the angle of inclination as shown in figure 8.

4.2. *Pinching instability*

The pinching instability is a mechanism by which the longitudinal roll planform decreases the wavenumber of longitudinal rolls for angles less than Θ_{cr}. This decrease in wavenumber occurs when two neighbouring roll pairs combine into a single larger-wavelength roll pair. A typical example of such a pinching sequence is shown in figure 17 (Plate 6). Most often the initial stages of the pinching mechanism are preceded by the breaking of a roll pair into two sections (figure 17*a*, *b*), after which the lower sections, following various transient motions, combine to form a longer-wavelength 'root' (figure 17*c*). This 'root' then pinches off the remaining two 'branches', as the longer wavelength 'root' elongates at the expense of the two smaller-wavelength 'branches' (figure 17*d*, *e*). This local process is then invariably followed by a global transient motion which readjusts the planform to an essentially uniform-wavenumber distribution (figure 17*f*). The pinching mechanism in a horizontal layer was exhibited experimentally by Busse & Whitehead (1971). Whitehead (1976) studies aspects of the Prandtl-number dependence of the pinching mechanism measuring the speed of progression of the pinch sequence in various silicon oils. In

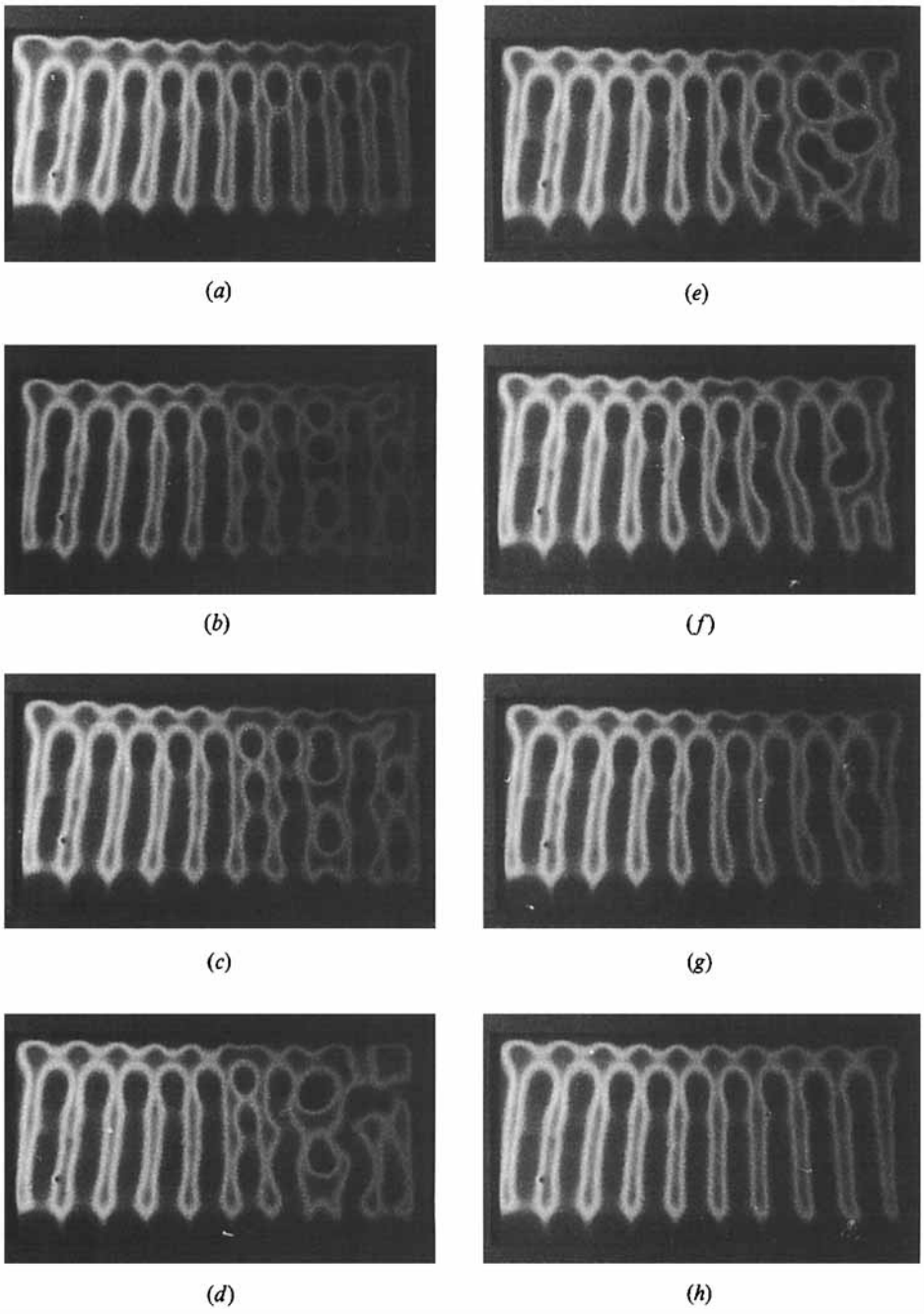

FIGURE 16. Loss of a roll pair by the cross-roll instability at 7.5°, $Ra^* = 10^4$, $(A_x, A_z) = (10, 20)$, run no. 700: (a) $t = 0$ min; (b) 22 min; (c) 23 min; (d) 25 min; (e) 30 min; (f) 32 min; (g) 35 min; (h) 40 min.

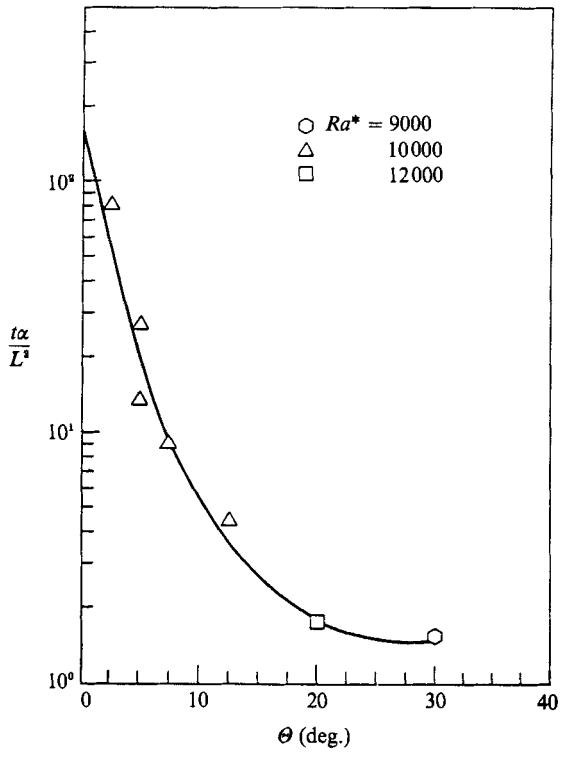

FIGURE 18. Effect of angle of inclination on transient rearrangement times for loss of a roll pair, $A_x, A_z = (10, 20)$.

large-aspect-ratio layers of silicone oil, they found processes similar to the above for the progression of the pinching instability.

The two wavelength-changing mechanisms discussed above have been observed mainly in runs where the angle of inclination is decreased from 90° to 0°. A similar mechanism for increasing the wavenumber of the longitudinal rolls is also observed in runs where Θ varied from 0° to 90°. In this case a longitudinal roll breaks in half (lengthwise), the upper portion then moves to the side of the original 'root' and becomes a stationary base. The two neighbouring half-rolls then elongate to form two complete roll pairs. Whether the true cross-roll or pinching mechanisms of wavelength modification are present in such situations is not apparent at this time.

4.3. *Rearrangement times for planforms*

The elapsed time necessary for the transient loss of a roll pair and the subsequent rearrangement to a steady-state planform at a lower angle is a strong function of the angle of inclination. At large Θ (figure 18) the time is about a vertical thermal diffusion time, L^2/α, whereas at low angles the elapsed time is about two orders of magnitude larger. Since $A_x = 10$ the elapsed time near the horizontal can be approximately scaled by $[W^2/\alpha]$. The controlling process of rearrangement for the layer is scaled (at least in the limiting cases) by the thermal diffusion of energy in the Y- and X-directions, at high and low angles of inclination respectively. At high angles thermal energy is transported mainly by convection in the X-direction and by conduction in the Y-direction. As the angle of inclination decreases, the upslope (X) component of gravity decreases in magnitude causing a decrease in the convective

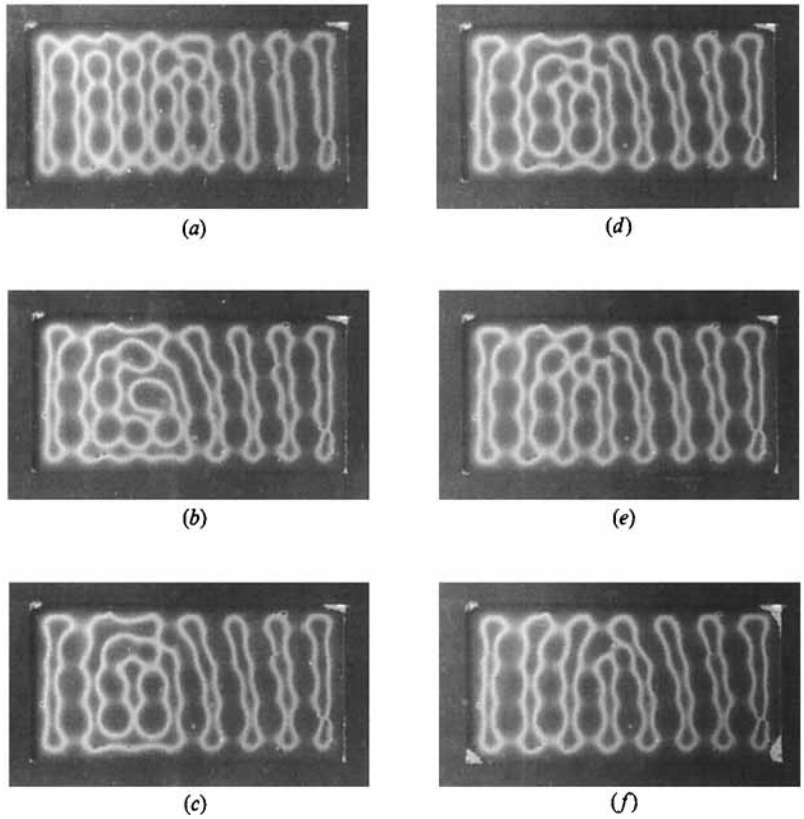

FIGURE 19. Loss of a roll pair by the cross-roll instability at 0°, $Ra^* = 10^4$, $(A_x, A_z) = (10, 20.5)$, run no. 125: (a) $t = 0$ min; (b) 40 min; (c) 75 min; (d) 90 min; (e) 3 h; (f) 12 h.

transport in the X-direction. The corresponding increase in the Y-component of gravity causes energy to be transported across the gap by convection with conduction in the much longer X-direction. Thus it appears that transient rearrangement elapsed times are determined by a thermal-diffusion-limited mechanism, with characteristic times (L^2/α) for large Θ and (W^2/α) for small Θ. The Z-direction contribution to this elapsed time may not be as significant because of the relatively strong convective transport taking place in the longitudinal roll pair. These roll pairs have a Z lengthscale of about $\lambda \approx 2L$, with thermal diffusion taking place between neighbouring roll pairs. This Z-direction thermal diffusion timescale appears not to alter the above order of magnitude estimates for rearrangement times. This scaling of rearrangement times could explain the necessity of long observation times in large-aspect-ratio horizontal enclosures when initially non-homogeneous planforms undergo a wavenumber rearrangement.

An example of such a transient rearrangment is shown in figure 19, where upon decreasing the angle to 0° the existing wavenumber of the newly formed square-cells is too large and the planform present becomes unstable. The cross-roll instability breaks up three columns of square cells which later, after rearrangement, form two such columns. A relatively short period of time ($\sim$ 60 min) is taken to break the pattern and replace it with the lower number of columns, while it appears that most of the time ($\sim$ 11 h) is used to develop columns (longitudinally, or X-direction) to

with the need to transport thermal energy in the longer X-direction by thermal diffusion.

5. Concluding remarks

The steady planforms and instability mechanisms present in an inclined enclosure with poorly conducting boundaries are in a number of situations similar to those in an enclosure with isothermal boundaries. At high angles of inclination, a transverse mode is stable; as the angle decreases this mode becomes unstable relative to a longitudinal roll planform which is qualitatively similar to those found with isothermal boundaries. The cross-roll mechanism observed with the (present) poorly conducting boundaries is similar to the cross-roll instability observed by Busse & Whitehead (1971) in a horizontal layer, and calculations by Clever & Busse (1977) for an inclined layer with isothermal boundaries. The pinching mechanism previously exhibited only in horizontal layers (Busse & Whitehead 1971) is found to be a quite common wavelength-changing mechanism in the poorly conducting case for inclined layers. Qualitatively, the unsteadiness at sufficiently high Ra^* appears to be similar to the wavy instability found by Hart (1971*a*, *b*), although a larger diversity of quasi-periodic motions is observed with the poorly conducting boundaries.

The observed planforms of convection for the poorly conducting case differ dramatically from the isothermal boundary case in the existence of square-cells at the horizontal, as was predicted by Busse & Riahi (1980), and Jenkins & Proctor (1984). The present visualization of square cells appears to confirm these calculations. In addition to the existence of square cells in the horizontal layer, enclosures with poorly conducting boundaries differ from those with isothermal boundaries at low angles of inclination. At these low angles, it appears that surface temperature fluctuations that are able to exist with a poorly conducting bounding surface stabilize the transverse modes of disturbances. This stabilization allows a steady transverse disturbance to exist superimposed on the longitudinal roll planform. This region of steady planforms is limited to low angles by the effect of the mean shear flow which tends to inhibit the transverse modes as the angle of inclination increases.

The liquid crystal/film heater technique provides good visualization and quantitative measurement of the temperature distribution on the lower bounding surface sustained by differing planforms of convective motion in inclined enclosures. The technique has allowed the observation of a number of transient dynamical processes used in planform rearrangement and wavenumber selection. In addition, unsteady quasi-periodic motions have been observed. The ability of the liquid crystal technique to visualize finite-amplitude disturbances has allowed the determination of an approximate stability map for a portion of the (Ra^*, Θ)-parameter space. A continued refinement of the experimental apparatus and procedure is underway. An extension of the present work is planned to investigate the characteristics of such poorly conducting surfaces at higher Ra^*.

The work reported here was supported in part by a grant from the National Science Foundation. Also, the help of Z. Johnson, B. Strozinksky and S. Olson in performing some of the experimental runs is gratefully acknowledged.

REFERENCES

BAUGHN, J. W., TAKAHASHI, R. K., HOFFMAN, M. A. & MCKILLOP, A. A. 1984 Local heat transfer measurements using an electrically heated thin gold-coated plastic sheet, *22nd Natl Heat Transfer Conference.*

BUSSE, F. M. 1978 Nonlinear properties of thermal convection. *Rep. Prog. Phys.*, **41**, 1929–1967.

BUSSE, F. M. 1981 Transition to turbulence in Rayleigh–Bénard convection. In *Hydrodynamic Instabilities and Transition to Turbulence* (ed. M. Swinney & J. Gollub). Springer.

BUSSE, F. M. & RIAHI, N. 1980 Non-linear convection in a layer with nearly insulating boundaries. *J. Fluid Mech.* **96**, 243–256.

BUSSE, F. M. & WHITEHEAD, J. A. 1971 Instabilities of convection rolls in a high Prandtl number fluid. *J. Fluid Mech.* **47**, 305–320.

CASTELLANO, J. & BROWN, G. 1973*a* Thermotropic liquid crystals, Part 1: The underlying science. *Chemtech* January.

CASTELLANO, J. & BROWN, G. 1973*b* Thermotropic liquid crystals, Part 2: Current uses and future ones, *Chemtech* January.

CHEN, M. M. & WHITEHEAD, J. A. 1968 Evolution of two-dimensional periodic Rayleigh convection cells of arbitrary wavenumbers. *J. Fluid Mech.* **31**, 1–15.

CLEVER, R. M. & BUSSE, F. M. 1977 Instabilities of longitudinal convection rolls in an inclined layer. *J. Fluid Mech.* **81**, 107–127.

DEGRAFF, J. G. A. & VAN DER HELD, E. F. M. 1953 *Appl. Sci. Res.* **A 3**, 393.

ENGELHART, R. & HEWGLEY, W. 1973 Thermal and Infrared Testing. In *Nondestructive Testing*, Chapter 6, *NASA Paper* SP-5113, GPO Stock Number 3300–00471.

FERGASON, J. 1968 Liquid crystal in nondestructive testing. *Appl. Optics* **7**, 1729–1737.

GOLDSTEIN, R. J. & FRANCHETT, M. E. 1988 Heat transfer from a flat surface to an oblique impinging jet. *Trans ASME* C: *J. Heat Transfer* **110**, 84–90.

GOLDSTEIN, R. J. & TIMMERS, J. F. 1982 Visualization of heat transfer from arrays of impinging jets. *Intl J. Heat Mass Transfer* **25**, 1857–1868.

HART, J. E. 1971*a* Stability of the flow in a differentially heated inclined box. *J. Fluid Mech.* **47**, 547–576.

HART, J. E. 1971*b* Transition to a wavy vortex regime in convective flow between inclined plates. *J. Fluid Mech.* **48**, 265–271.

HART, J. E. 1983 A note on the stability of low-Prandtl-number Hadley circulations. *J. Fluid Mech.* **132**, 271–281.

HASSAB, M. A. & OZISIK, M. N. 1981 Effects of thermal wall resistance on the stability of the condition regime in an inclined narrow slot. *Intl. J. Heat Mass Transfer* **24**, 739–747.

HIPPENSTEELE, S. H., RUSSELL, L. M. & STEPKA, F. S. 1981 Evaluation of a method for heat transfer measurements and thermal visualization using a composite of a heater element and liquid crystals. *ASME* 81-GT-93, *NASA Tech. Mem.* 81369.

HURLE, D. T. J., JAKEMAN, E. & PIKE, E. R. 1967 On the solution of the Bénard problem with boundaries of finite conductivity. *Proc. R. Soc. Lond.* A **296**, 469–475.

JENKINS, D. R. & PROCTOR, M. R. E. 1984 The transition from roll to square-cell solutions in Rayleigh–Bénard convection. *J. Fluid Mech.* **139**, 461–471.

KOSCHMIEDER, E. L. 1974 Bénard convection. *Adv. Chem. Phys.* **25**, 177–211.

OZISIK, M. N. & HASSAB, M. A. 1979 Effects of convective boundary conditions on the stability of conduction regime in an inclined slender slot. *Numer. Heat Transfer* **2**, 251–260.

PALM, E. 1975 Nonlinear thermal convection. *Ann. Rev. Fluid Mech.* **7**, 39–61.

RIAHI, N. 1985 Nonlinear thermal convection with finite conducting boundaries. *J. Fluid Mech.* **152**, 113–123.

SIMONICH, J. R. & MOFFAT, R. 1982 New technique for mapping heat-transfer coefficient contours. *Rev. Sci. Instrum.* 678–683.

SPARROW, E. M., GOLDSTEIN, R. J. & JONSSON, V. K. 1964 Thermal instability in a horizontal fluid layer: effect of boundary conditions and non-linear temperature profile. *J. Fluid Mech.* **18**, 513–528.

WHITEHEAD, J. A. 1976 The propagation of dislocations in Rayleigh–Bénard rolls and bimodal flow. *J. Fluid Mech.* **75**, 715–720.